34th Annual International Conference of the IEEE EMBS
San Diego, California USA, 28 August - 1 September, 2012

Automatic Brain MR Images Diagnosis Based on Edge Fractal Dimension and Spectral Energy Signature

Salim Lahmiri and Mounir Boukadoum

Abstract—**A new automatic system to detect pathologies in human brain magnetic resonance (MR) images is presented. The goal is to classify normal versus abnormal images affected by Alzheimer, Glioma, Herpes, Metastatic, and Multiple Sclerosis. The extracted features are the fractal dimension of edges in the Hilbert domain, and the skewness and kurtosis of their spectral energy distribution. The proposed system (FDSE) outperforms the popular discrete wavelet transform (DWT) and principal component analysis (PCA).**

I. Introduction

A number of automated diagnosis systems have been proposed for classifying normal versus abnormal brain tissue based on two-dimensional magnetic resonance (MR) images [1]-[3]. MR images can provide high-resolution anatomical details and reliable early detection of pathologies at the beginning stages is essential for developing appropriate treatments. Most works on MR image classification use the discrete wavelet transform (DWT) as the first step of feature extraction. Thanks to the DWT's property of preserving both the time and frequency dimensions of the input signal while allowing a scaled view of the signal [3], it has been successfully applied to brain MR images to extract textural features for classification. For instance, Chaplot et al. [1] used the Daubechies-4 wavelet decomposition at level two to extract low-low frequency (approximation) coefficients to be fed to support vector machines (SVM). The radial basis function and polynomial function were used as kernels for non-linear training and testing. The dataset consisted of fifty-two brain MR images of which six normal and forty-six abnormal, of brain affected by Alzheimer's disease. Four normal images and six abnormal images were randomly chosen for training the SVM and forty-two images were used for testing. The obtained correct classification rate was 98% for both types of kernels. El-Dahshan et al. [2] applied principal component analysis (PCA) to the DWT's low-low frequency image. In this case, a 3rd level DWT decomposition was performed, with Haar wavelets used to extract the low frequency coefficients. Then, the first seven principal components were kept to form the features vector fed to the classifier, namely the backpropagation artificial neural network (BPNN) trained with Levenberg-Marquardt numerical algorithm and the *k*-nearest neighbor (*k*-NN). The dataset included ten normal images and sixty abnormal images of Glioma, Metastatic bronchogenic carcinoma, Alzheimer's disease, and visual agnosia. The learning and test set size were not indicated. The correct classification rates obtained by BPNN and *k*-NN were 97% and 98%, respectively. Zhang et al. [3] also applied Haar wavelets and third-level decomposition to extract the low frequency coefficients. Then, PCA was applied to obtain the first nineteen principal components, thus preserving 95.4% of the total variance of the low frequency image. The obtained principal components were sent to a BPNN trained with scaled conjugate gradient (SCG) for classification. The initial dataset consisted of 18 normal and 48 abnormal images of Glioma, Meningioma, Alzheimer, Alzheimer plus visual Agnosia, Pick's disease, Sarcoma, and Huntington's disease. The data were randomly divided into two equal-size learning and test sets and the obtained correct classification rates on both training and test images were 100%. Cross validation was ignored in all the previous studies.

In this paper, we present a new approach based on fractal geometry and the spectral energy distribution of edges (patterns/object boundaries) in brain MR images for detecting those pathologies that manifest themselves as regions of brightness change in the cerebral tissue. Because edges represent abrupt changes in image brightness, their distributions in normal and abnormal brain MR images may be different, and we propose to distinguish normal from abnormal anatomical silhouettes in human brain MR images by means of their fractal dimensions and spectral signatures. The goal is to compare our approach with the DWT-PCA in the most recent work [3] where 100% correct classification rate was reported.

The paper is organized as follows. Section 2 provides more details about our methodology; Section 3 presents the data and displays the simulation results; a conclusion along with future direction is drawn in section 4.

II. Methodology

The Hilbert transform [4] is applied to the brain MR image for analysis purpose. The advantage of the Hilbert transform is that it does not require a predetermined origin and baseline [5] and is a viable approach to display the time-frequency structure of non stationary signals [6]. Then, a Sobel filter [7] is applied to the Hilbert transformed image to detect edges. Given MR images with high intensity contrast regions, the Sobel filter which is based on first-order differentials could provide strong edge strength at the brain boundaries affected by those pathologies. Other edge detectors such as Laplacian and Canny's operator could be considered, but the former may lead to false detections and the latter requires parameter tuning [8]. The extracted edges are analyzed by means of fractal and power spectrum signatures to extract features. The fractal of the image is

Mounir Boukadoum is full professor in the department of computer science at the University of Quebec at Montreal. C.P. 8888, Succ. C.-V., Montreal (Quebec), H3C 3P8 Canada (e-mail: boukadoum.mounir@uqma.ca).

Salim Lahmiri is PhD candidate in the same department (e-mail: lahmiri.salim@courrier.uqam.ca).

determined by the fractal dimension (FD) derived from the power-law scaling [9][10] and measures the irregularity of edges. In addition, two high order statistics, namely the skewness and kurtosis of the spectral energy distribution of the Sobel processed image, are computed to form the image feature vector with FD. Indeed, since a normal human brain MR image appears to be symmetric, we make the hypothesis that skewness and kurtosis are suitable to account for symmetry. Finally, the features vector is fed to a BPNN trained by the scaled conjugate numerical algorithm as in [3]. The diagram of our system (FDSE) is shown in Figure 1, whilst the standard system based on DWT and PCA [2][3] is shown in Figure 2.

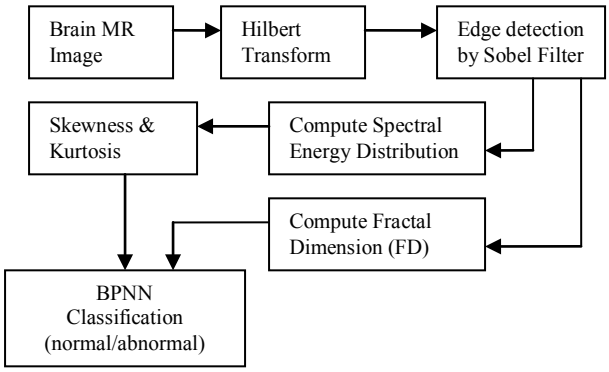

Figure 1. Diagram of the FDSE system.

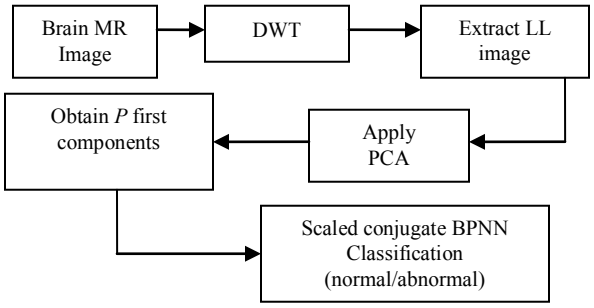

Figure 2. Diagram of the DWT-PCA system as in [2][3].

We also followed the DWT-PCA methodology described in [3] (see Figure 2) as an alternative way to extract features from our image database. This was done to assess the effectiveness of our methodology in comparison. As in [3], we used the Haar wavelet as mother function and set the level of DWT decomposition to three. Using PCA, we extracted the p principal components (features) that preserved ninety-five percent of total variance to be fed to the BPNN trained with scaled conjugate gradient numerical algorithm. As in [3], p was found to be nineteen.

As for the details of our screening system (FDSE), they are presented below.

A. Hilbert transform

The Hilbert transform [4][6] of a signal $x(t)$ is defined as:

$$H[x(t)] = \frac{1}{\pi}\int_{-\infty}^{+\infty}\frac{x(t)}{t-\tau}d\tau \quad (1)$$

It we represent the edges of $x(t)$ with a staircase function, it can be shown that their locations correspond to the singularities of $H[x(t)]$ manifested by its extrema [7]. These could be determined by processing the magnitude of the analytic signal $x_a(t) = x(t) + jH[x(t)]$, or by using amplitude thresholding. In this work, a Sobel filter is used to extract the edge image, after transforming the original one by applying the Hilbert transform to each column. Thus, the Sobel filter is applied to $H[x(t)]$.

B. Sobel filter

The Sobel filter [8] processes the obtained Hilbert image for edge detection. It does so by measuring the gradient of the image intensity at each pixel, using two 3×3 differentiation matrices (kernel Sobel filters) along the horizontal (moving right) and vertical directions (moving down). Then, each pixel of the obtained images provides the x or y axis component of the gradient and the image edges can be derived from the distribution of the gradient amplitude, defined as:

$$S = \sqrt{S_x^2 + S_y^2} \quad (2)$$

where,

$$S_x = \begin{bmatrix} -1 & 0 & +1 \\ -2 & 0 & +2 \\ -1 & 0 & +1 \end{bmatrix} * I \text{ , and } S_y = \begin{bmatrix} -1 & -2 & -1 \\ 0 & 0 & 0 \\ +1 & +2 & +1 \end{bmatrix} * I \quad (3)$$

and the * operator denotes two-dimensional convolution.Figures 2 and 3 provide examples of original MR images and their Sobel-filtered versions.

C. Fractal Dimension

The fractal dimension (FD) measures the degree of complexity of a geometric shape. There exist many ways to define it [10][11]. The most popular ones define FD as the exponent of a power law between the number of fragments obtained by splitting the shape into pieces and the shape reduction factor used to obtain them. For instance, the fractal dimension of a 2-D image would be the exponent obtained by splitting the image into blocs and relating their number to the split factor used (self-similarity method). Alternatively, the image can be placed on a grid whose x axis resolution is varied and, each time, the number of boxes that the image occupies in the grid is counted. Then, the slope of the best-fit Log-Log straight line between these two variables is computed to yield the fractal dimension (box counting method). The box-counting technique is adopted in this paper for simplicity and because it is more generic (it also applies to non self-similar shapes). Following this technique, the fractal dimension of an image structure (edge) is given by:

$$FD = \lim_{r\to 0}\left[\frac{\log(N(r))}{\log\left(\frac{1}{r}\right)}\right] \quad (4)$$

where, r is the box size scale factor and $N(r)$ is the number of boxes used to cover the edge of the image. By varying the box size, FD is estimated by least-squares regression fitting of $\log(N(r))$ against $\log(1/r)$.

D. Spectral Energy Distribution

Based on the Fourier transform [12], spectral analysis allows detecting high-energy bursts in the image spectrum. For a given $M \times N$ digital image $f(x,y)$, the discrete Fourier spectrum $|F(u,v)|$ is computed as [12]:

$$|F(u,v)| = \frac{1}{MN}\sum_{x=0}^{M-1}\sum_{y=0}^{N-1} f(x,y)\exp\left(-j2\pi\left(\frac{ux}{M}+\frac{vy}{N}\right)\right) \quad (5)$$

where $u = 0,1,\ldots, M\text{-}1$ and $v = 0,1,\ldots, N\text{-}1$. Then, the spectral energy distribution $S(\theta)$ of the Fourier spectrum for each radial direction θ is given by:

$$S(\theta) = \sum_{r=1}^{R} s(r,\theta) \quad (6)$$

where $s(r,\theta)$ is the Fourier spectrum $|F(u,v)|$ in polar coordinates with $u = r\cdot\cos(\theta)$ and $v = r\cdot\sin(\theta)$, r being the radius of a circle centered at the origin of the two-dimensional spectrum and θ an angle varying between 0 and 180°. $S(\theta)$ is a one-dimensional signal from which high order statistics, namely skewness and kurtosis, will be computed. The results are then combined with the fractal dimension to form the feature vector.

D. The classifier

As in [3], the feature vector is fed to a BPNN [13] trained with the scaled conjugate gradient (SCG) algorithm [14] for final image classification and comparison purpose. The SCG was chosen by the authors in [3] because it is considerably faster than standard conjugate gradient methods. This is because the SCG algorithm is based on conjugate directions but does not perform a line search at each iteration t. For instance, the weights w of the network are updated as follows:

$$w(t+1) = w(t) + \lambda(t)\cdot d(t) \quad (7)$$

where d is the search direction and λ is the step size which minimize the function $f(w(t)+\lambda(t)\cdot d(t))$. The step size is computed as follows [14]:

$$\lambda(t) = -\frac{d(t)^T \nabla f(w(t))}{d(t)^T H\, d(t) + \gamma(t)\|d(t)\|^2} \quad (8)$$

where H is the Hessian matrix and $\gamma \geq 0$. More technical details about the algorithm and its parameters are given in [14]. The number of neurons in both the input layer and hidden layer was set to the number of features: nineteen for the DWT-PCA approach and three for the FDSE approach. The transfer function in the hidden layer was the tangent sigmoid. All input data were scaled to [-1, 1] prior to learning.

III. DATA AND SIMULATION RESULTS

The database consisted of ten normal brain MR images and fifty six abnormal images that corresponded to Alzheimer (13), Glioma (12), Herpes (8), Metastatic Bronchogenic Carcinoma (9), and Multiple Sceloris (14). All the images were T2-weighted of 256×256 size, obtained from the Harvard Medical School webpage [15]. Figures 3 and 4 show examples as well as the effect of Sobel filtering them in the Hilbert domain and of computing their spectral energy distribution (from which skewness and kurtosis are computed).

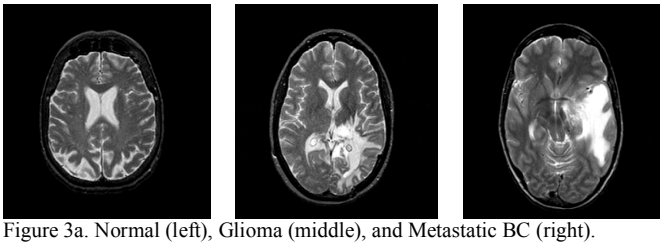

Figure 3a. Normal (left), Glioma (middle), and Metastatic BC (right).

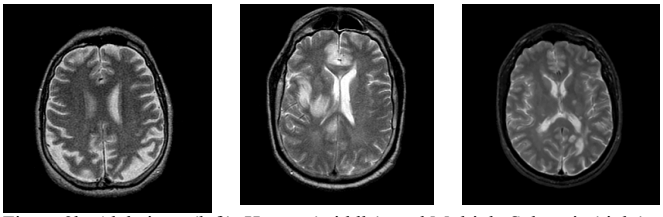

Figure 3b. Alzheimer (left), Herpes (middle), and Multiple Sclerosis (right).

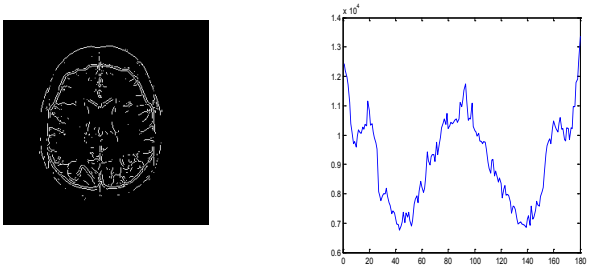

Figure 4. Sobel filtered image in Hilbert domain (left) and its spectral energy distribution (right). Example of a normal image.

Ten experiments were conducted with the data being randomly divided into two equal-size learning and test sets each time (in contradistinction with [3] where only one trial was conducted), with the goal to evaluate the average accuracy of the backpropagation neural network. In each experiment, the performance of BPNN was evaluated by finding the average correct classification rate. Then, the total average correct classification rate and its standard deviation were computed. The classification results are given in Table 1. They indicate that the approach based on the fractal dimension and skewnes and kurtosis of the edges' spectrum energy distribution achieves 91.78% correct classification rate against 82.69% obtained by the DWT-PCA described in [3]. In addition, the standard deviation of our approach (0.0148) is substantially lower than that of the DWT-PCA approach (0.0796), which shows a better generalization

capability. The fact that we only obtained 82.69% accuracy in comparison to the 100% reported in [3] could be due to our use of cross validation and the fact that we did not use exactly the same pathologies. In Table 2, we give the correct classification rate (CCR), specificity and sensitivity when the BPNN is trained to classify normal image against only one type of pathology. The results obtained with DWT-PCA are given in parenthesis. As one can see, the proposed features perform better than the standard approach for all pathologies; in particular, we obtained 100% accuracy for normal versus Multiple Sclerosis, and 96% accuracy for normal versus Alzheimer's disease.

Table 1. Correct classification rate: normal against all.

	FDES	DWT-PCA
Average	91.78%	82.69%
Standard deviation	0.0148	0.0796

Table 2. Simulation results: normal against one.

	Alz	Glioma	Herpes	Meta.	Sclerosis
CCR	96 (86)	83 (80)	80 (77)	83 (79)	100 (92)
Specificity	95 (77)	90 (68)	70 (68)	77 (57)	100 (88)
Sensitivity	100 (100)	57 (87)	90 (80)	78 (92)	100 (85)

In our study, normal images are positive samples and abnormal images are negative samples. Therefore, according to specificity statistics (correctly classified negative samples over true negative samples), our approach performs better that the DWT-PCA in detecting all negative samples. The difference is particularly striking for Alzheimer (95%) and Glioma (90%). On the other hand, we obtained mixed results for sensitivity statistics (correctly classified positive samples over true positive samples). In this case, DWT-PCA preformed better for Metastatic (92%) and Glioma (87%), and FDSE equally well or better for the other pathologies..

The better overall performance of the proposed approach could be due to the following causes: First, the DWT-PCA approach is based on the analysis of the biological tissue by means of multi resolution pixel analysis with a predetermined mother wavelet and level of decomposition. The choice of the wavelet and level of decomposition could have an impact on the effectiveness of the extracted features. On the other hand, the Hilbert transform requires no predetermined filter or level of analysis. Second, PCA relies on a transformation that performs a linear projection; thus, it fails to capture a nonlinear distribution of pixels in the original feature space. Third, since a normal human brain MR image appears to be symmetric, the skewness and kurtosis computed from the spectral signature of edge and fractal dimension are all suitable to account for asymmetry in the images. For instance, the fractal dimension assesses the complexity of a geometric form and, thus, helps to quantifying multi convoluted patterns in brain MR images.

IV. CONCLUSION

In this work, a comparison is made for detecting pathologies in brain MR images between two feature extraction techniques, one based on image compression with the two-dimensional discrete wavelet transform and subsequent dimension reduction with principal component analysis (DWT-PCA), and the edge fractal dimension and spectral energy signature (FDSE). The classification results obtained with a feedforward neural network with error backpropagation training (BPNN), trained with the scaled conjugate gradient algorithm show that the FDSE-based diagnosis system outperforms the popular approach based on DWT-PCA for accuracy. They also show that extracting features from edges leads to better generalization capability in comparison to textural features. The classification accuracy could be improved further by replacing the BPNN classifier by support vector machines (SVM; work in progress) and a larger database would probably lead to more improvement in generalization capability.

REFERENCES

[1] S. Chaplot, L.M Patnaik, and N.R. Jagannathan, "Classification of magnetic resonance brain images using wavelets as input to support vector machine and neural network," *Biomedical Signal Processing and Control*, vol. 1, pp. 86-92, 2006.

[2] E.-S.A. El-Dahshan, T. Hosny, and A.-B.M. Salem, "Hybrid intelligent techniques for MRI brain images classification," *Digital Signal Processing*, vol. 20, pp. 433-441, 2010.

[3] Y. Zhang, Z. Dong, L. Wu, and S. Wang, "A hybrid method for MRI brain image classification," *Expert Systems with Applications*, vol. 38, pp. 10049-10053, 2011.

[4] N.E. Huang, Z. Shen, and S.R. Long, "A new view of water waves – The hilbert spectrum, " *Annu. Rev. Fluid Mech*., vol. 3, pp. 417-457, 1999.

[5] R. Green and J.M. Stanley, "Application of a Hilbert transform Method to The Interpretation of Surface-Vehicule Magnetic Data," *Geophysical Prospecting*, vol. 23 (1), pp. 18-26, 2006.

[6] E. Oruklu, Y. Lu, and Jafar Saniie, "Hilbert Transform Pitfalls and Solutions for Ultrasonic NDE Applications," in *Proc. IEEE International Ultrasonics Symposium Proceedings*, Roma, 2009, pp.2004-2007.

[7] G.M. Livadas and A.G. Constantinides, "Image edge detection and segmentation based on the Hilbert transform," in *Proc. IEEE Internat. Conf. Acoust. Speech Signal Process*, New York, 1988, vol. 2, pp. 1152-1155.

[8] M. Sonka, *Image Processing Analysis and Computing Vision*. Brooks/Cole, 2001.

[9] E. Meinhardt, E. Zacur, A.F. Frangi, and V. Caselles, "3D edge detection by selection of level surfaces patches," Journal *of Mathematical Imaging and Vsion*, vol. 34, pp. 1-16, 2009.

[10] B.B. Mandelbrot, *Fractal Geometry of Nature*. New York: W H. Freeman Freeman & Co. 1983.

[11] R. Lopes and N. Betrouni, "Fractal and multifractal analysis: A review," *Medical Image Analysis*, 13, pp.634-649, 2009.

[12] R.C. Gonzalez and R.E. Woods, *Digital Image Processing*. 3rd ed., Prentice Hall, 2008.

[13] M.F. Møller, "A scaled conjugate gradient algorithm for fast supervised learning," *Neural Networks*, vol. 6, no. 4, pp. 525–533, 1993.

[14] S. Haykin, *Neural Networks and Learning Machines*. 3rd Ed., Prentice Hall; 2008.

[15] http://med.harvard.edu/AANLIB/